Materials Chemistry and Physics 135 (2012) 1064–1069

Contents lists available at SciVerse ScienceDirect

Materials Chemistry and Physics

journal homepage: www.elsevier.com/locate/matchemphys

Multisite luminescence of rare earth doped TiO_2 anatase nanoparticles

Željka Antić [a], Radenka M. Krsmanović [a], Marko G. Nikolić [a], Milena Marinović-Cincović [a], Miodrag Mitrić [a], Stefano Polizzi [b], Miroslav D. Dramićanin [a,*]

[a] Vinča Institute of Nuclear Sciences, University of Belgrade, P.O. Box 522, 11001 Belgrade, Serbia
[b] Università Ca' Foscari Venezia, Dipartimento di Scienze Molecolari e Nanosistemi, Via Torino, 155b I-30172 Mestre, Italy

HIGHLIGHTS

- ► Sm^{3+}, Eu^{3+} and Tb^{3+} are incorporated into anatase nanocrystals via sol–gel route.
- ► Sm^{3+} and Eu^{3+} luminescence originate from 3 different sites in TiO_2 nanocrystals.
- ► Details on multisite structure for Sm^{3+} doped TiO_2 are presented for the first time.

GRAPHICAL ABSTRACT

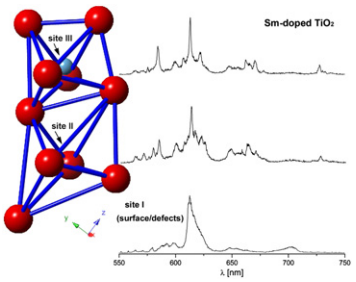

ARTICLE INFO

Article history:
Received 12 October 2011
Received in revised form
26 April 2012
Accepted 13 June 2012

Keywords:
Nanostructures
Optical materials
Photoluminescence spectroscopy
Optical properties

ABSTRACT

Eu^{3+}, Sm^{3+} and Tb^{3+} ions have been incorporated into anatase TiO_2 nanocrystals via hydrolytic sol–gel method. Pure anatase phase was confirmed with XRD and TEM measurements. Band gap energies change slightly with rare earth incorporation, from 3.32 eV for undoped TiO_2 to 3.15 eV, 3.25 eV and 3.29 eV for Tb^{3+}, Sm^{3+} and Eu^{3+} doped TiO_2. Photoluminescence of Eu^{3+} and Sm^{3+} originated from three different sites in TiO_2 nanocrystals have been identified with the laser-excited site-selective spectroscopy measurements at 10 K. One site exhibits broad emission peaks, which are ascribed to the distorted lattice site near the surface. Other two sites, associated with the inner lattice, show significantly sharper fluorescence lines as a consequence of an ordered crystalline environment. The emission decays of Eu^{3+} and Sm^{3+} have similar values for inner-lattice sites and longer lifetimes for near-surface sites. The luminescence of Tb^{3+} doped TiO_2 nanocrystals was immeasurably weak.

1. Introduction

Titanium (IV)-oxide occurs in nature in three mineral forms: anatase, brookite and rutile. All three phases are characterized with high refractive index ($n_{anatase}$ = 2.488, n_{rutile} = 2.609, $n_{brookite}$ = 2.583), low absorption and low dispersion in visible and near-infrared spectral regions, high chemical and thermal stabilities. This important metal-oxide semiconductor with relatively wide band gap (3.25 eV for anatase, 3.0 eV for rutile, 1.9 eV for brookite) [1] and low phonon energy (<700 cm^{-1}) is an excellent host for various rare earth (RE) impurities providing their efficient emission in visible range [2–6]. These systems are of possible interest in white light emission diode (LED) industry [7–10] and as photocatalysts [11,12]. At the same time, being non-toxic and biocompatible, rare-earth doped anatase has strong potential to replace standard types of fluorophores (quantum dots, organic dyes, etc.), traditionally used as fluorescent markers in medicine and biological applications [13].

In particular anatase phase is considered very promising and has been widely investigated for various applications in lithium-ion batteries, filters, waveguides, anti-reflective and highly reflective coatings [14–19], but it still remains a challenge to keep this phase

* Corresponding author. Tel.: +381 11 3408 191; fax: +381 11 3408 607.
E-mail address: dramican@vinca.rs (M.D. Dramićanin).

0254-0584/$ – see front matter © 2012 Elsevier B.V. All rights reserved.
http://dx.doi.org/10.1016/j.matchemphys.2012.06.016

stable from easy transformation to rutile. Setiawati and Kawano [20] studied the stabilization of anatase phase with Eu^{3+} and Sm^{3+} ions, added in different concentration, ranging from 0.1 to 1 mol%. They claimed that the significant suppression of TiO_2 nanoparticle growth and stabilization of anatase phase were achieved by RE doping, getting better results for higher dopant concentrations.

Following these findings, we decided to produce anatase nanoparticles via sol–gel method and to use as dopants Eu^{3+}, Sm^{3+} and Tb^{3+} ions, adding them in concentration of 3 at.%. We documented the successful synthesis of stable and pure anatase phase through several experiments: basic characteristics of synthesized materials from thermal analysis (TG/DTA), X-ray diffraction (XRD), Fourier transmission infrared (FTIR), scanning and transmission electron microscopy (SEM and TEM), nitrogen sorption measurements, UV–vis and photoluminescence (PL) spectroscopy, and discussed obtained results. Using site-selective technique at low temperature (10 K) we were able to prove the incorporation of RE^{3+} ions into the TiO_2 lattice. The existence of three nonequivalent sites of Eu^{3+} and Sm^{3+} in anatase matrix has been reported and discussed.

2. Materials and methods

2.1. Synthesis

To produce anatase TiO_2 in the form of nanopowder the hydrolytic sol–gel route has been adopted, starting from rare-earth nitrates and titanium (IV)-isopropoxide. The sol–gel technology offers several processing advantages as the starting materials are mixed at the nanoscale level. In this way a complete and controlled mixing of components is ensured at the preliminary stage, the reaction rate is increased and the processing temperature lowered.

For synthesis of undoped and 3 at.% Eu^{3+}, Sm^{3+} and Tb^{3+} doped TiO_2, titanium (IV)-isopropoxide (Alfa Aesar), water, ethanol and nitric acid were mixed in molar ratio of 1:3:20:0.08 [21]. In the first step, titanium (IV)-isopropoxide was dissolved in ethanol under constant magnetic stirring. For doped samples stoichiometric quantities of Eu_2O_3, Sm_2O_3 and Tb_2O_3 (Alfa Aesar, 99.9%) were dissolved in appropriate amount of HNO_3 and water, and added to titanium (IV)-isopropoxide/ethanol mixure. For undoped sample only appropriate amount of HNO_3 and water was added. Transparent gels were obtained within few minutes and dried at 70 °C for 5 h under atmospheric pressure. Then samples were heated at 5 °C min^{-1} heating rate up to 210 °C and held at that temperature for 20 min, with further calcination at 420 °C for 2 h. The calcination procedure is chosen after TG/DTA analysis, which results are presented in the Section 3.

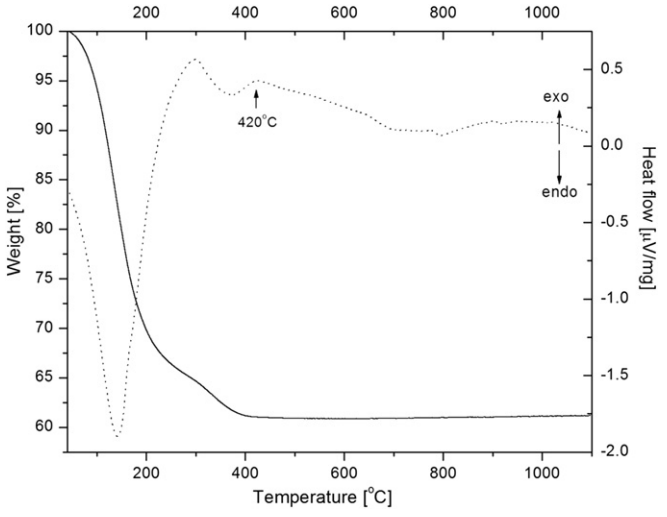

Fig. 1. Thermogravimetry (TG, solid line) and differential thermal analysis (DTA, doted line) curves for undoped TiO_2 gel prepared via hydrolytic sol–gel method.

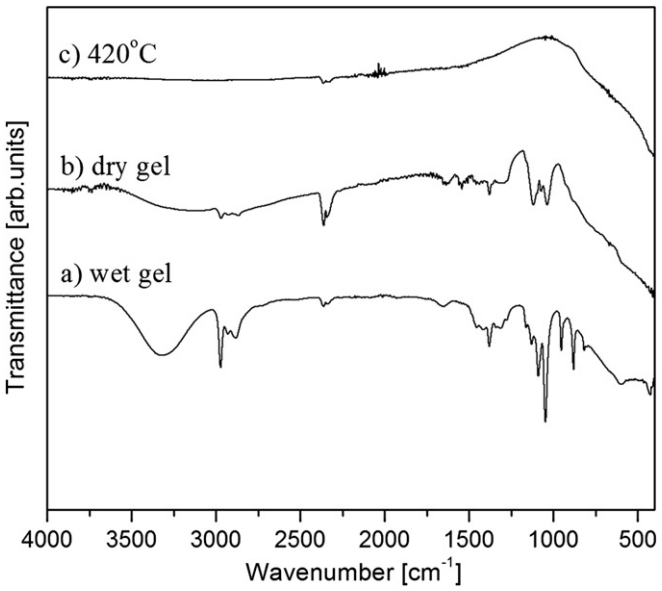

Fig. 2. FTIR spectra of undoped a) wet and b) dry TiO_2 gel and c) TiO_2 powder calcinated at 420 °C for 2 h.

2.2. Measurements

TG/DTA analysis were performed on the SETARAM SETSYS Evolution-1750 instrument. The gel of undoped anatase (~10–15 mg), taken before drying and annealing, was heated at 10 °C min^{-1} heating rate, in air atmosphere (air flow 16 ml min^{-1}), from 30 to 1000 °C. Fourier transmission infrared (FTIR) measurements were carried out on the Thermo Nicolet 380 FT-IR instrument, in a reflection mode with a resolution of 4 cm^{-1}.

XRD patterns were collected using a Philips PW 1050 with Ni filtered Cu $K_{\alpha 1,2}$ radiation ($\lambda = 0.154$ nm) in a 2θ range from 10° to 120°, counting for 8 s in 0.05° steps. Microstructure at local level was observed via JEOL 3010 transmission electron microscope

Table 1
Characteristic vibrational modes obtained from FTIR measurements.

Functional group	Region	Comments
TiO_2 network bonds	Below 1000 cm^{-1}	Continuous absorption
O–H stretching vibrations	3600–3000 cm^{-1}	Water and isopropanol
O–H deformation vibrations	~1430–1370 cm^{-1}	From isopropanol
Aliphatic C–H stretching vibration	3000–2800 cm^{-1}	From isopropanol
Asymmetrical CH_3 deformation vibrations	~1450 cm^{-1}	From isopropanol
Symmetrical CH_3 deformation vibration	~1380 cm^{-1}	From isopropanol
$-CH(CH_3)_2$ skeletal vibrations	~1170–880 cm^{-1}	From isopropanol
C–O stretching vibration	~1090 cm^{-1}	From isopropanol
O–N=O asymmetrical stretching	~1650 cm^{-1}	From nitrates
N–O stretching vibrations	~800 cm^{-1}	From nitrates
O–N=O deformation vibration	~600 cm^{-1}	From nitrates
CO_2	~2400–2300 cm^{-1}	Inevitable in the atmosphere

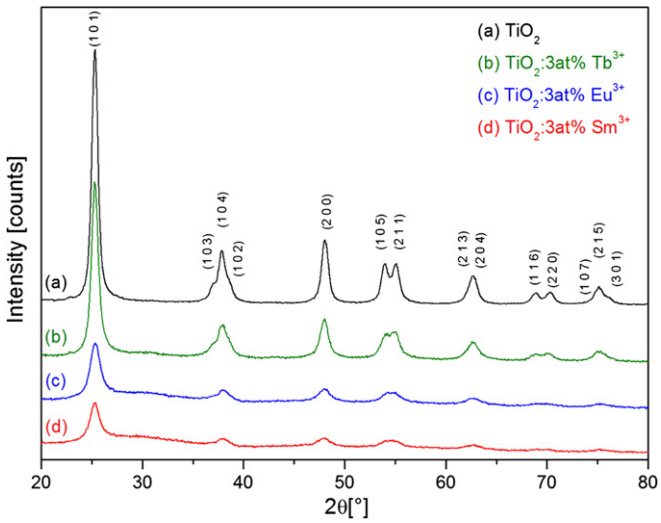

Fig. 3. XRD patterns of undoped and RE^{3+} doped TiO_2 anatase nanopowders; the most pronounced reflections are indexed according to JCPDS card no. 21-1272 (anatase TiO_2).

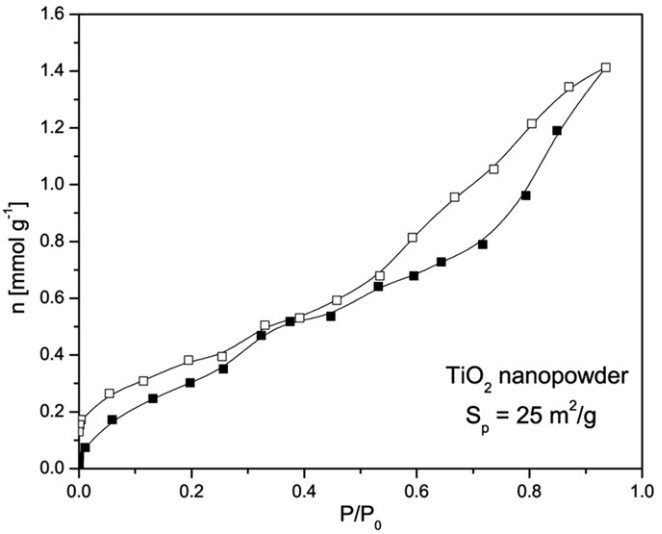

Fig. 5. Nitrogen adsorption isotherms, for the amount of N_2 adsorbed as function of relative pressure for pure TiO_2 nanopowder. Solid symbols – adsorption, open symbols – desorption.

(TEM). Adsorption and desorption isotherms of N_2 were measured at −196 °C using the gravimetric McBain method. The specific surface area (S_{BET}) was calculated from isotherms according to Brunauer, Emmett and Teller (BET) equation. Diffuse spectral reflectance measurements were done for the spectral range 300–625 nm, on the Thermo Evolution 600 spectrometer equipped with integrating sphere, using $BaSO_4$ as a blank.

For low temperature measurements samples were mounted on a closed cycle cryostat (10–350 K, DE202AE Advanced Research Systems) attached to a high resolution spectrofluorometer system which comprises optical parametric oscillator excitation source (EKSPLA NT 342, emission range 210–2300 nm) and spectrograph FHR 1000 (Horiba Jobin-Yvon), and ICCD detector (Horiba Jobin-Yvon). The line intensities and positions of the measured spectra were calibrated with a standard mercury–argon lamp.

Diffuse reflectance and photoluminescence measurements were performed on pellets prepared from the powders under a load of 5 tons and without any additives.

3. Results and discussion

The TiO_2 gels prepared with hydrolytic sol–gel method were of amorphous nature and under appropriate sintering they transformed to crystalline TiO_2. In order to determine proper sintering temperature needed for the transformation to anatase phase, we performed a thermal analysis of the synthesized gels. Results of TG/DTA analysis clarified the existence of three temperature regions (see Fig. 1): i) the DTA endothermic peak between room temperature and 300 °C, which can be attributed to the vaporization of adsorbed water and organic molecules, while the TG curve in the same temperature range shows a marked weight loss (∼35%); ii) the second weight loss indicated by TG (∼5%) and the endothermic effect indicated by DTA, observed in the temperature range between 300 °C and 400 °C, may be related to the elimination of the residual organic compounds; iii) the exothermic peak at 420 °C could be attributed to the transformation of amorphous titania gel to the crystalline anatase TiO_2 phase, while the mass remains constant after 400 °C.

Fig. 2 shows the FTIR spectra of wet and dry TiO_2 gels and of the powder obtained after calcinations at 420 °C for 2 h. The continuous absorption, visible in all samples below 1000 cm^{-1}, can be attributed to the TiO_2 network bonds [22]. Water and alcohol content, especially in the wet gel, is marked as a broad peak in the region of 3600–3000 cm^{-1} [22]. As expected, this peak was much weaker in dry gel and disappeared completely after the final thermal treatment. Many peaks in the gels' spectra are due to the organic and nitrate presence (see Table 1) and they became weaker

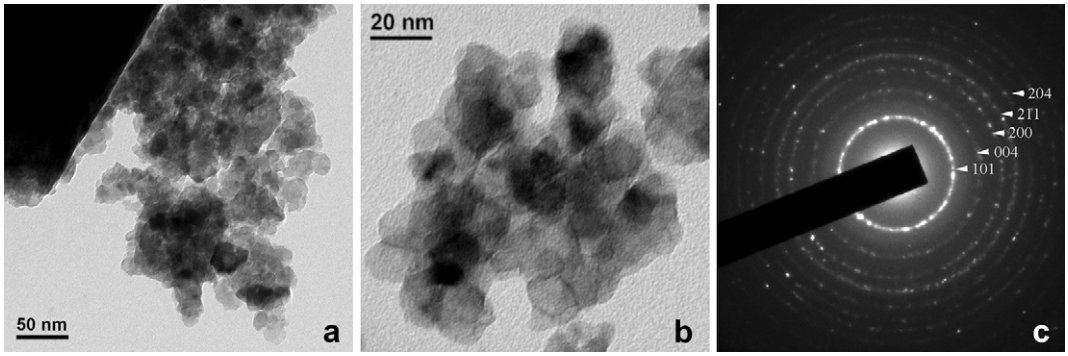

Fig. 4. Representative TEM images of a) TiO_2 powder agglomerate and b) closer look to its nanoparticles; c) corresponding electron diffraction pattern with marked Miller indices of anatase TiO_2.

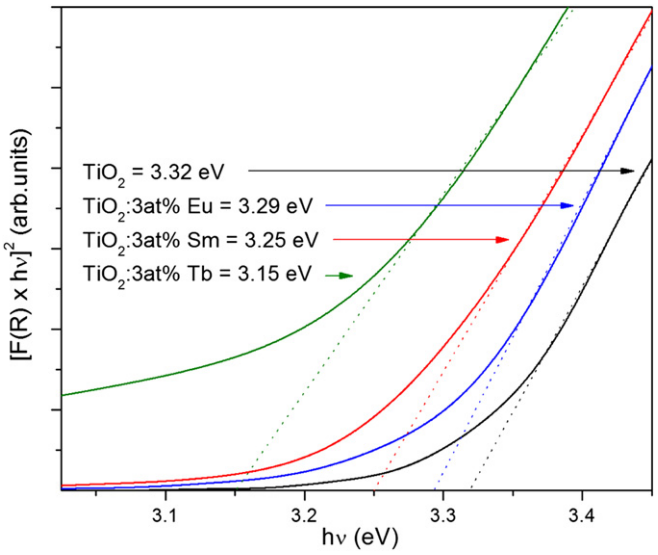

Fig. 6. Optical band gaps for undoped TiO_2 and TiO_2 doped with Eu^{3+}, Sm^{3+} and Tb^{3+}, provided from extrapolation of the $(\alpha_{KM}h\nu)^2$ plot given as a function of photon energy E.

or completely disappeared after drying. After firing at 420 °C only the TiO_2 absorption below 1000 cm^{-1} and the CO_2 peaks are recognizable.

Titanium-oxide crystallizes in three forms: anatase (tetragonal), brookite (orthorhombic) and rutile (tetragonal), all containing six coordinated titanium ion. Anatase and brookite are low-temperature forms, and upon heating over 600 °C they start the conversion to rutile. In Fig. 3 XRD patterns of undoped and RE^{3+} doped TiO_2 nanopowders (undoped sample – black line, Tb^{3+} doped – green line, Eu^{3+} doped – blue line, and Sm^{3+} doped – red line) are presented. The most pronounced peaks are indexed according to the JCPDS card No. 21-1272 which corresponds to the pure anatase phase. Detailed inspection of diffractograms showed no evidence of rutile or brookite traces in any of the prepared samples. Anatase TiO_2 crystallizes in a tetragonal structure, space group $I4_1/amd$ (No. 141). In this structural type titanium ions have special crystallographic positions 4a with local symmetry $\bar{4}2m(D_{2d})$ while oxygen ions have special crystallographic positions 8e with local symmetry *mm*. This structure can be visualized in terms of chains of TiO_6 octahedra, where each Ti^{4+} ion is surrounded by an octahedron of six O^{2-} ions and each octahedron is in contact with eight neighbors (four sharing a corner and four sharing an edge). Depending on the doping concentration trivalent rare earth ions may substitute Ti^{4+} ions at their sites in anatase lattice, segregate in separate phase, or may occupy interstitial sites in some cases. Analysis of diffraction peaks according to Scherrer's equation, performed on (101) reflections, showed that TiO_2 particle crystallite size is about 14 nm for undoped powder and 9 nm, 6 nm and 5.8 nm for powders doped with Tb^{3+}, Eu^{3+} and Sm^{3+}, respectively. The reduction of anatase particle crystallite coherent sizes after doping with RE ions has been already reported in the literature [23,24] and can be attributed to the presence of RE–O–Ti bonds that inhibit the growth of crystal grains. Incorporation of larger ions ($r_{Tb(III)} = 100.9$ pm, $r_{Eu(III)} = 103.6$ pm, $r_{Sm(III)} = 108.6$ pm >> $r_{Ti(IV)} = 68$ pm, in octahedral coordination, data taken from www.webelements.com) into TiO_2 causes the increase of the unit cell and induces disorder into the lattice. Increase of the unit cell is manifested through a very small shift of the reflection peaks toward smaller angles.

Widening of reflection peaks at higher diffraction angles reveals induced lattice disorder after doping. The (1 0 5) and (2 1 1) reflection peaks at 2θ around 54.5°, as well as (1 1 6) and (2 2 0) at around 70°, are well resolved for undoped sample (see Fig. 4) while in doped samples these peaks merge in one with more pronounced effect for larger dopant ions. It is worth mentioning that doping with trivalent rare earth ions induces charge imbalance in the TiO_2 crystal structure. For the studied dopant concentration there is no traces of segregate phases that could be observed from the XRD measurements.

TEM observations show that TiO_2 powder has dense aggregates made up of crystalline nanoparticles of about 10–20 nm in size for the maximum dimension (Fig. 4a and b). The local crystal structure of anatase was confirmed by selected area electron diffraction (SAED) technique; one SAED ring diffraction pattern with marked Miller indices of anatase TiO_2 (JCPDS card no. 21-1272) is given in Fig. 4c. The ring pattern confirmed that our material is polycrystalline, while the grainy appearance of rings is related to the fact that the constituent crystallites have a size of 10 nm or more.

Nitrogen adsorption isotherms, presenting the amount of N_2 adsorbed as a function of relative pressure at −196 °C, are shown in Fig. 5. According to the IUPAC classification [25] isotherms are of type IV. Specific surface area calculated by BET equation, S_{BET}, is determined to be 25 $m^2\ g^{-1}$.

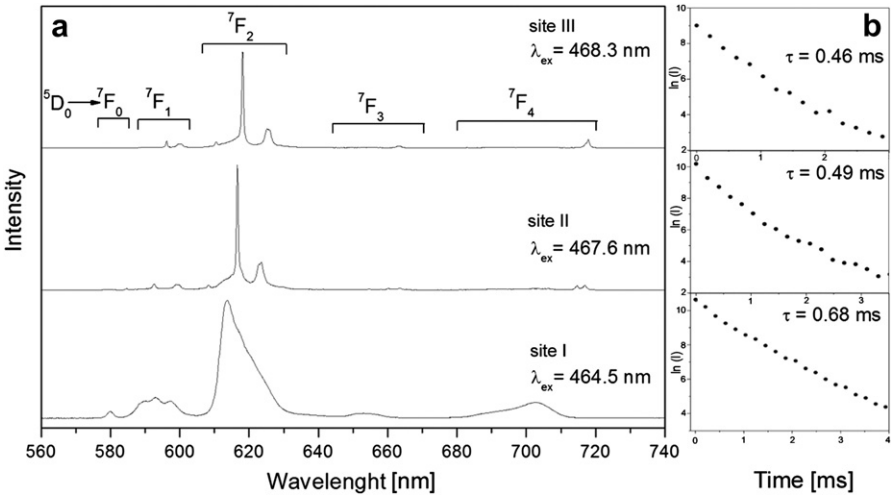

Fig. 7. a) Emission spectra of TiO_2:Eu^{3+} measured at 10 K obtained for three sites: I (excited at 464.5 nm), II (excited at 467.6 nm) and III (excited at 468.3 nm) and b) corresponding emission decay curves.

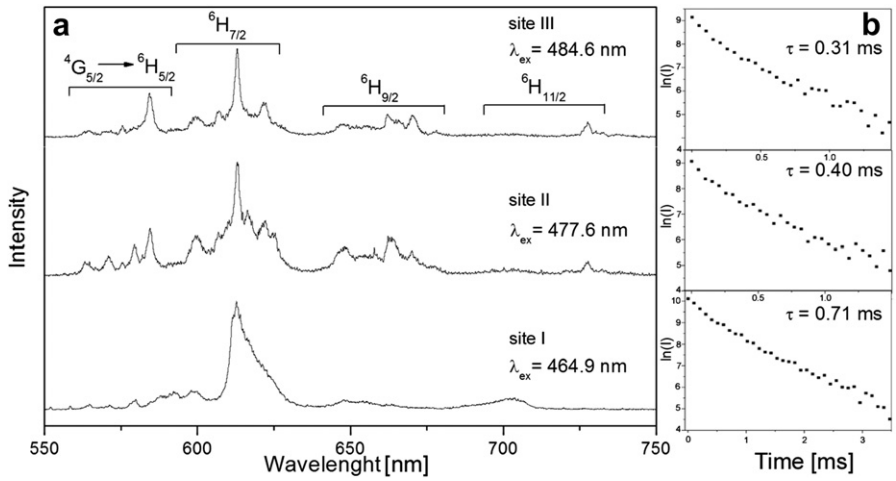

Fig. 8. a) Emission spectra of TiO_2:Sm^{3+} measured at 10 K obtained for three sites: I (excited at 464.9 nm), II (excited at 477.6 nm) and III (excited at 484.6 nm) and b) corresponding emission decay curves.

The UV/vis reflectance spectra of undoped and RE^{3+} doped TiO_2 nanocrystalline powders are used to estimate energy band gaps. $[F(R) \times h\nu]^2$ versus $h\nu$ (indirect semiconductor band gap) in the vicinity of absorption edge are plotted for all samples in Fig. 6. $F(R)$ is the Kubelka–Munk function [26,27] defined as $F(R) = (1-R)^2/2R$, $h\nu$ is photon energy and R is measured reflectance. By the extrapolation of the linear part of the curve to the intersect with x-axes one can assess band gap energies of 3.32 eV for undoped and 3.15 eV, 3.25 eV and 3.29 eV for Tb^{3+}, Sm^{3+} and Eu^{3+} doped TiO_2, respectively. The results correspond well to those reported in the literature for anatase nanoparticles [28]. The small decrease in band gap values for rare earth doped nanocrystals may hardly be ascribed to quantum confinement effect (even though reduction of particle size is evidenced after rare earth ions incorporation) since particle sizes exceed the Bohr radius by a factor of 4 [29]. The possible explanation could be a slight modification of materials density of states after incorporation of trivalent rare earth ions [30].

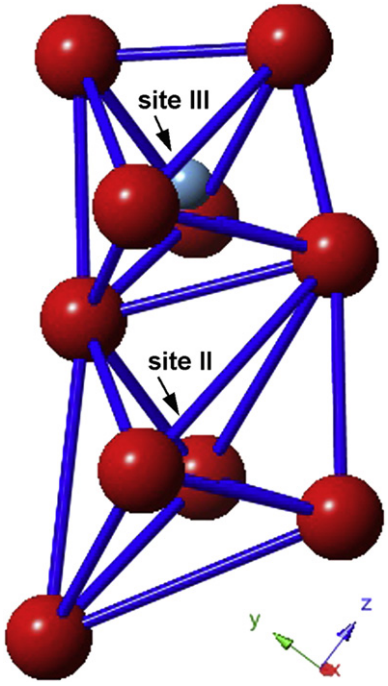

Fig. 9. Schematic representation of the sites II and III local environment in TiO_2 anatase structure.

Photoluminescence emission properties of rare earth doped TiO_2 is investigated by means of laser excited high resolution site-selective spectroscopy at low temperature (10 K) and emission decay measurements. Emission from multiple sites is evidenced for Eu^{3+} and Sm^{3+} doped samples, shown in Figs. 7a and 8a, respectively. Neglected emission is found for Tb^{3+} doped sample, which was expected since Tb^{3+} excited states have larger energy than the trap levels of anatase nanocrystals [31].

The multisite structure of Eu^{3+} in anatase nanocrystals was first evidenced by Luo et al. [32] and Liu et al. [33]. However, in the case of Er^{3+} doped anatase only one single lattice site emission is found by the same authors [33]. Our results on multisite emission of Eu^{3+} doped anatase (Fig. 7) confirm reported findings in [32,33] (number of sites and site symmetries) and the same three-site structure has been proved for Sm^{3+} doped TiO_2 sample (see Fig. 8). Photoluminescence spectra are composed of characteristic emission bands of trivalent Eu^{3+} ($^5D_0 \rightarrow {}^7F_0$, $^7F_1$, $^7F_2$, $^7F_3$ and $^7F_4$) and Sm^{3+} ($^4G_{5/2} \rightarrow {}^6H_{5/2}$, $^6H_{7/2}$, $^6H_{9/2}$ and $^6H_{11/2}$) ions (see Figs. 7a and 8a). According to branching and selection rules [34] one may conclude that incorporation of larger ions and charge imbalance reduces site symmetry from D_{2d} to C_1 for site I, to C_{2v} for site II and D_2 for site III, for both Eu^{3+} and Sm^{3+} doped anatase nanocrystals. Emission spectra from the lowest symmetry site I are quite broadened and can be related to distorted sites near nanoparticle's surface or other defects. Spectra from other two sites (site II and site III) are composed of sharp emission lines, suggesting a crystalline environment for rare earth ions (of strong covalency) and their incorporation into nanoparticle volume. Schematic representation of the sites II and III is given in Fig. 9.

In undoped anatase both sites have similar environment, being inside the scalenohedrons, with local symmetry $\bar{4}2m$ (D_{2d}). Titanium ion could occupy the site in the smaller scalenohedron (site III, volume 9.45 Å^3) or the vacancy in the larger scalenohedron (site II, volume 13.26 Å^3). After incorporation of large RE^{3+} ions these sites reduce symmetries (remaining in the same symmetry group) due to distortions. The environment of smaller site III takes disphenoidal geometry (D_2 local symmetry), while the larger site II takes pyramidal geometry (C_{2v} local symmetry).

The PL excitation spectrum of Eu^{3+} and Sm^{3+}-doped TiO_2 samples with marked transitions, measured in the spectral region between 350 and 550 nm at room temperature, are displayed in Fig. 10. In the spectrum of Eu-doped sample (Fig. 10a) four excitation bands could be identified and attributed to the direct

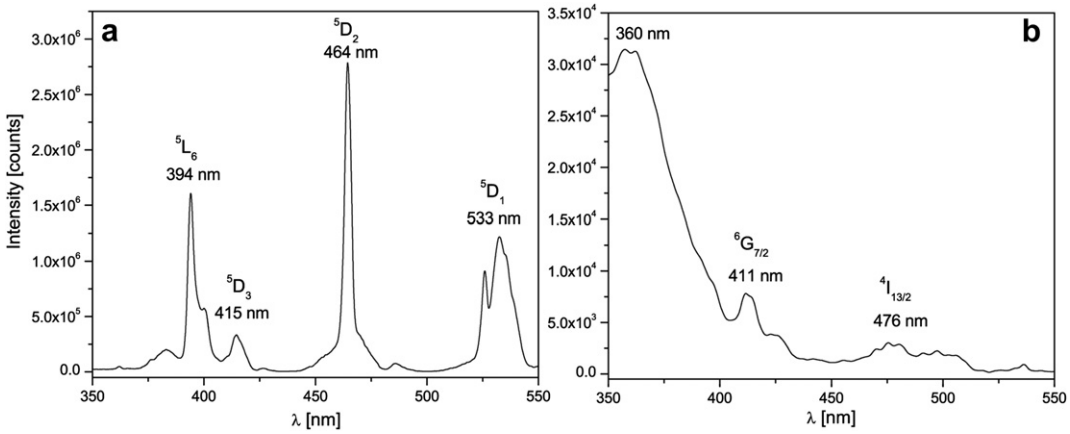

Fig. 10. Excitation spectra of a) TiO_2:Eu^{3+} (λ_{em} = 613 nm) and b) TiO_2:Sm^{3+} (λ_{em} = 612 nm) measured at room temperature.

excitation of Eu^{3+} ions to the $^5L_6$ (394 nm), $^5D_3$ (415 nm), $^5D_2$ (464 nm) and $^5D_1$ (533 nm) levels. The excitation spectrum of Sm-doped sample (Fig. 10b) exhibits the most pronounced band centered at ~360 nm, associated with the band-to-band excitation of TiO_2 and the following energy transfer to Sm^{3+} ions, indicating that the sensitized excitation is more efficient than the direct one [8,31]. Other two, less pronounced excitation bands, centered at 411 and 476 nm, could be attributed to the direct excitation of Sm^{3+} ions to the $^6G_{7/2}$ and $^4I_{13/2}$ levels, respectively [8,35].

Recorded emission decays (see Figs. 7b and 8b) exhibit a pure single exponential behavior excluding the possibility of decays' superposition from different sites. Lifetime values are found to be 0.68 ms, 0.49 ms and 0.46 ms in the case of Eu^{3+} and 0.71 ms, 0.40 ms and 0.31 ms in the case of Sm^{3+}, for sites I, II and III, respectively. It is interesting to note that emission lifetime from disordered site, both for Eu^{3+} and Sm^{3+}, is longer than lifetime from higher symmetry sites II and III. Eu^{3+} emission decays are slightly higher compared to the previous findings [32].

4. Conclusions

Thermal and infrared analysis revealed the typical behavior of materials produced by sol–gel, with removal of residual water and solvents at lower temperatures and organic compounds at higher ones, as well as the formation of crystalline anatase phase. Purity of the anatase phase in all studied samples has been confirmed through XRD measurements, and at the local level with TEM observations. The small decrease in band gap values is noted for rare earth doped nanocrystals and could be ascribed to slight modification of materials density of states induced by rare earth ions. We did not detect any luminescence from the Tb^{3+}-doped sample, while characteristic red emission has been observed in Eu^{3+} and Sm^{3+}-doped samples. PL laser-excited site-selective spectroscopy measurements at low temperature provided a clear evidence of Eu^{3+} and Sm^{3+} ions incorporation into anatase matrix. For both samples the existence of three different emission centers for RE ions impurities is confirmed.

Acknowledgments

Authors acknowledge the financial support of the Ministry of Education and Science of the Republic of Serbia (45020).

References

[1] R. Zallen, M.P. Moret, Solid State Commun. 137 (2006) 154–157.
[2] V. Kiisk, I. Sildos, S. Lange, V. Reedo, T. Tätte, M. Kirm, J. Aarik, Appl. Surf. Sci. 247 (2005) 412–417.
[3] C.C. Ting, S.Y. Chen, W.F. Hsieh, H.Y. Lee, J. Appl. Phys. 90 (2001) 5564.
[4] R. Palomino-Merino, A. Conde-Gallardo, M. García-Rocha, I. Hernández-Calderón, V. Castaño, R. Rodríguez, Thin Solid Films 401 (2001) 118–123.
[5] A. Conde-Gallardo, M. García-Rocha, R. Palomino-Merino, M.P. Velásquez-Quesada, I. Hernández-Calderón, Appl. Surf. Sci. 212-213 (2003) 583–588.
[6] C. Urlacher, J. Mugnier, J. Raman. Spectrosc. 27 (1996) 785–792.
[7] S. Lange, I. Sildos, V. Kiisk, J. Aarik, Mat. Sci. Eng. B-Solid 112 (2004) 87–90.
[8] V. Kiisk, V. Reedo, O. Sild, I. Sildos, Opt. Mater. 31 (2009) 1376–1379.
[9] C. Gao, H. Song, L. Hu, G. Pan, R. Qin, F. Wang, Q. Dai, L. Fan, L. Liu, H. Liu, J. Lumin. 128 (2008) 559–564.
[10] C. Jia, E. Xie, A. Peng, R. Jiang, F. Ye, H. Lin, T. Xu, Thin Solid Films 496 (2006) 555–559.
[11] M. Bettinelli, A. Speghini, D. Falcomer, M. Daldosso, V. Dallacasa, L. Romanò, J. Phys. Condens. Matter. 18 (2006) S2149.
[12] M. Venkatachalam, V. Palanichamy, Murugesan, Mater. Chem. Phys. 104 (2007) 454–459N.
[13] L. Li, C.K. Tsung, Z. Yang, G.D. Stucky, L.D. Sun, J.F. Wang, C.H. Yan, Adv. Mater. 20 (2008) 903–908.
[14] F. Wu, X. Li, Z. Wang, H. Guo, L. Wu, X. Xiong, X. Wang, J. Alloys Compd. 509 (2011) 3711–3715.
[15] D.J. Kim, S.H. Hahn, S.H. Oh, E.J. Kim, Mater. Lett. 57 (2002) 355–360.
[16] Z. Wang, U. Helmersson, P.O. Käll, Thin Solid Films 405 (2002) 50–54.
[17] D. Grosso, P.A. Sermon, Thin Solid Films 368 (2000) 116–124.
[18] Z.W. Zhao, B.K. Tay, S.P. Lau, G.Q. Yu, J. Cryst. Growth 268 (2004) 543–546.
[19] A. Bendavid, P.J. Martin, Å. Jamting, H. Takikawa, Thin Solid Films 355–356 (1999) 6–11.
[20] E. Setiawati, K. Kawano, J. Alloys Compd. 451 (2008) 293–296.
[21] G. Dagan, M. Tomkiewicz, J. Phys. Chem. 97 (1993) 12651–12655.
[22] G. Socrates, Infrared and Raman Characteristic Group Frequencies - Tables and Charts, third ed., J. Wiley & Sons, Chichester, 2001.
[23] F.B. Li, X.Z. Li, M.F. Hou, Appl. Catal. B Environ. 48 (2004) 185–194.
[24] V. Stengl, S. Bakardjieva, N. Murafa, Mater. Chem. Phys. 114 (2009) 217–226.
[25] K.S.W. Sing, Pure Appl. Chem. 57 (1985) 603–619.
[26] L. Yang, B. Kruse, J. Opt. Soc. Am. A 21 (2004) 1933–1941.
[27] L. Yang, S.J. Miklavcic, J. Opt. Soc. Am. A 22 (2005) 1866–1873.
[28] N.D. Abazović, M.I. Čomor, M.D. Dramićanin, D.J. Jovanović, S.P. Ahrenkiel, J.M. Nedeljković, J. Phys. Chem. B 110 (2006) 25366–25370.
[29] U. Hörmann, U. Kaiser, M. Albrecht, J. Geserick, N. Hüsing, J. Phys. Conf. Ser. 209 (2010) 012039.
[30] M.G. Brik, I. Sildos, V. Kiisk, Physica B 405 (2010) 2450–2456.
[31] K.L. Frindell, M.H. Bartl, M.R. Robinson, G.C. Bazan, A. Popitsch, G.D. Stucky, J. Solid State Chem. 172 (2003) 81–88.
[32] W. Luo, R. Li, G. Liu, M.R. Antonio, X. Chen, J. Phys. Chem. C 112 (2008) 10370–10377.
[33] Y. Liu, W. Luo, H. Zhu, X. Chen, J. Lumin. 131 (2011) 415–422.
[34] J.C.G. Bünzli, V. Eliseeva, in: P. Hänninen, H. Härmä (Eds.), Lanthanide Luminescence: Photophysical, Analytical and Biological Aspects, Springer-Verlag, Berlin Heidelberg, 2011, p. 39.
[35] E. De la Rosa-Cruz, L.A. Diaz-Torres, P. Salas, R.A. Rodriguez, G.A. Kumar, J. Appl. Phys. 94 (2003) 3509–3515.